

The Nature and Role of Bridged Carbonyl Intermediates in the Ultrafast Photo-induced Rearrangement of $\text{Ru}_3(\text{CO})_{12}$

Elizabeth A. Glascoe, Matthias F. Kling,[‡] Jennifer E. Shanoski, and Charles B. Harris^{}*

Contribution from the Department of Chemistry, University of California, Berkeley, California 94720,
and Chemical Sciences Division, Lawrence Berkeley National Laboratory, Berkeley, California 94720

**RECEIVED DATE (to be automatically inserted after your manuscript is accepted if required
according to the journal that you are submitting your paper to)**

^{*} E-mail: cbharris@berkeley.edu

[‡] Present address: FOM Institute for Atomic and Molecular Physics (AMOLF), Kruislaan 407, 1098 SJ Amsterdam, The Netherlands.

ABSTRACT

The photochemistry of the trimetal cluster, $\text{Ru}_3(\text{CO})_{12}$, was investigated on the ultrafast timescale using UV-vis pump, infrared probe spectroscopy in order to study the transient intermediates formed upon photoexcitation. The dynamics of these intermediates can only be unambiguously identified by monitoring the small but distinct infrared absorptions of bridging carbonyls. The nature and role of bridged carbonyl intermediates in the photochemistry of $\text{Ru}_3(\text{CO})_{12}$ in both coordinating and non-coordinating solvents is discussed. In an inert solvent such as cyclohexane, photoexcitation of $\text{Ru}_3(\text{CO})_{12}$ with 400 nm light produces two different species that have never been observed simultaneously. The first species is a carbonyl loss complex with a bridged carbonyl that forms in 134 ± 22 ps and survives beyond 800 ps; the second species is a bridged carbonyl complex with one metal-metal bond cleaved that forms in 23 ± 3 ps and has a lifetime of 60 ± 5 ps. When 266 nm light was used to photoexcite the cluster, both species exhibit similar dynamics. This is the first time multiple bridged carbonyl intermediates have been observed simultaneously for this cluster and this observation resolves an inconsistency in the literature. Interestingly, in neat solutions of THF only one feature was observed in the bridging carbonyl region, yet the dynamics of the feature and density functional theory (DFT) results indicate that there are, in fact, two bridging carbonyl complexes with overlapping bands. These results were surprising as it was previously unknown whether THF would block formation of bridging carbonyl complexes by solvating and stabilizing the coordinatively unsaturated metal.

KEYWORDS Metal Carbonyl Complexes, Infrared Spectroscopy, Triruthenium Dodecacarbonyl, Photochemistry, Density Functional Theory

I. Introduction

The transition metal cluster $\text{Ru}_3(\text{CO})_{12}$ is widely used in photo-activated synthesis and therefore its rearrangement and decomposition dynamics are not only of fundamental interest but also of industrial importance.^{1,2} In general, photo-activation of this cluster allows for systematic control in synthetic procedures by breaking only specific types of bonds in the complex when a particular wavelength of light is used.^{2,3} A particularly interesting aspect of this system is that it exhibits unique dynamics, due to its trimetal infrastructure, that are not possible in corresponding metal monomers or dimers. The structure of $\text{Ru}_3(\text{CO})_{12}$ and of some of its photochemical intermediates, as well as the main reaction channels, have been investigated previously in matrices and solutions using laser flash photolysis in combination with visible or infrared spectroscopy.⁴⁻¹³ It is evident from a thorough examination of previous studies that many fundamental aspects, including the wavelength specificity of bond cleavage and the nature of the transients formed, are unclear. The ambiguity in the current picture for $\text{Ru}_3(\text{CO})_{12}$ reactivity prompted an investigation of this reaction using spectroscopic techniques that allow for detection of transient species with high sensitivity and ultrafast time resolution.

Previous experimental analysis and theoretical modeling indicated that $\text{Ru}_3(\text{CO})_{12}$ has a triangular arrangement of the metal atoms with four terminal carbonyl groups attached to each metal (see Figure 1, starting complex).^{5,11} The UV-vis spectrum has two prominent absorption bands, the first centered at 390 nm and the second centered at 238 nm. Electronic absorption studies indicate that the lower energy band (390 nm) of $\text{Ru}_3(\text{CO})_{12}$ originates from $\sigma^* \leftarrow \sigma$ transitions in metal d-orbitals,^{14,15} so that excitation with visible light in this region results in heterolytic cleavage of one of the Ru-Ru bonds.^{6,12,16} The complex formed retains the three metal cluster unit and exhibits a bridged carbonyl to accommodate the redistribution of charge (see Figure 1, complex I). This bridged carbonyl transient and its dynamics have been characterized in a previous study using ultrafast infrared spectroscopy, by its signature bridged carbonyl stretching frequency of ca. 1850 cm^{-1} .¹³ The subsequent photochemistry has been extensively studied, and it is generally observed that the solvent plays a key role in determining the final photoproducts (see Figure 1, long λ irradiation).^{6-8,16} In non-coordinating solvents, i.e. solvents that are

not able to stabilize the intermediate, such as alkanes, it is observed that the starting material is eventually reformed.^{6,16} In the presence of π -backbonding ligands, for example CO and phosphines, fragmentation of the photoexcited cluster and formation of three identical monomer units each containing a π -backbonding molecule is observed.^{6-8,16} Interestingly, in the presence of molecules, such as THF, that can only donate electron density to the metal in a σ -bonding fashion, photofragmentation is blocked and the starting material is regenerated; the reasons for this behavior remain unclear.⁶⁻⁸

The short wavelength, high energy peak at 238 nm in the UV-vis absorption spectrum of $\text{Ru}_3(\text{CO})_{12}$ has been characterized as a metal to ligand charge transfer (MLCT) excitation that ultimately results in loss of one carbonyl group in solution or in a matrix.^{3,14} Again, the solvent molecules play a key role in determining the final photoproducts. Non-coordinating solvents such as alkanes cannot stabilize the coordinatively unsaturated cluster so the complex is internally stabilized by a bridging carbonyl between two of the metal atoms (Figure 1, complex **II**). The bridged carbonyl has been observed in a 90 K matrix and in solution in the 1830-1850 cm^{-1} region.^{3,10} In coordinating solvents, both σ -donating and π -backbonding, the solvent molecule binds and forms the photo-substituted product $\text{Ru}_3(\text{CO})_{11}\text{S}$ (S = solvent molecule). The lifetime of this product depends on its thermodynamic stability with respect to the starting material and the availability of CO to replace the solvent S and reform the original cluster.^{3,7-9}

Despite the wealth of information provided by previous studies, some particularly important details of the photochemistry of $\text{Ru}_3(\text{CO})_{12}$ are unresolved. First, the timescales of formation and decay for the CO loss transient have not been determined and the structures of both bridged carbonyl complexes discussed above are uncertain. Second, a clear picture of the structure and dynamics of the cluster in σ -donating solvents does not exist. Finally, a careful perusal of the literature exposes an inconsistency concerning the number and type of photoproducts formed with disparate wavelengths of excitation as is discussed below. Photofragmentation products are formed upon excitation with both visible and ultraviolet light (in the presence of π -backbonding ligands) and a constant quantum yield between 313 and 436 nm was observed.^{7,8,16} In contrast, the quantum yields for photosubstitution products resulting

from excitation in this spectral region tend to decrease dramatically with decreasing wavelength.^{7,8} The pathways for the generation of two different products that are formed at the same wavelength remain unexamined. It has been suggested that photofragmentation is a result of the photochemistry that starts with photodissociation of a carbonyl.¹⁰ It was hypothesized by others that both the carbonyl loss channel and the metal-metal cleavage channel are accessed at all wavelengths in this region.^{7,8}

Most studies have suggested that a bridged carbonyl complex (regardless of whether it is derived from the CO loss or metal-metal cleavage channel) is formed in non-coordinating solvents.^{6-8,16} A few studies have directly observed a bridged carbonyl complex, and each study used a different wavelength of excitation.^{3,10,13} It is important to point out that in every study in which a bridged carbonyl complex was observed, only one species could be detected. This is inconsistent with results that suggest multiple photoproducts, derived from multiple bridged carbonyl complexes, are formed at a single excitation wavelength.^{7,8} In addition, different vibrational frequencies were reported for the bridging carbonyl in each study, possibly due to experimental limitations of wavelength resolution and detection sensitivity. Despite all the previous work to characterize the photochemistry of $\text{Ru}_3(\text{CO})_{12}$, the structure and number of bridged carbonyl complexes formed at various excitation wavelengths remains in dispute.

We investigated the primary photoproducts of $\text{Ru}_3(\text{CO})_{12}$ excited at 266 and 400 nm in solutions of cyclohexane and THF using a combination of ultrafast infrared absorption spectroscopy and DFT modeling. The goal of this study was to gain a more complete understanding of the transient photoproducts formed upon UV and visible excitation of $\text{Ru}_3(\text{CO})_{12}$. In contrast with previous studies, we were able to spectroscopically resolve all relevant bridging carbonyl intermediates and have found that two types of bridged carbonyl complexes are in fact present after both 266 nm and 400 nm excitation. What follows is a clearer picture of the ultrafast dynamics of the cluster upon photoexcitation that resolves inconsistencies in the literature and clarifies open questions on the photochemistry of transition metal clusters.

The paper is organized as follows: experimental and theoretical methods are described in Sect. II, the results on the photochemistry of $\text{Ru}_3(\text{CO})_{12}$ in cyclohexane and THF solution after 266- and 400-nm

irradiation are given in Sect. IIIA and the DFT calculations are presented in Sect. IIIB. In section IV, the dynamics of the photoexcited clusters with non-coordinating and coordinating solvents is discussed. We finally conclude our results on the photochemistry of $\text{Ru}_3(\text{CO})_{12}$ in Sect. V.

II. Methods

A. Samples

$\text{Ru}_3(\text{CO})_{12}$, spectroscopic grade cyclohexane and anhydrous THF were purchased from Sigma-Aldrich and used without further purification. Dilute solutions (1-2 mM) were prepared and filtered.

B. Femtosecond infrared spectroscopy

The experimental apparatus has been described in detail elsewhere.¹⁷ In brief, the setup consists of a Ti:sapphire regenerative amplifier (SpectraPhysics, Spitfire) seeded by a Ti:sapphire oscillator (SpectraPhysics, Tsunami) to produce a 1-kHz train of 100-fs pulses centered at 800 nm with an average pulse power of 0.9 mJ. The output of this system is split and used to generate 266- (0.3 μJ at sample) or 400-nm (1.6 μJ at sample) pump pulses and to pump a homebuilt optical parametric amplifier (OPA) able to deliver mid-IR probe pulses tunable from 3.0 – 6.0 μm with a spectral width of 200 cm^{-1} and a pulse duration of around 150 fs. A computer controlled translation stage (Klinger) allows for variable time delays up to 800 ps between pump and probe pulses.

The sample is flowed using a mechanical pump through a stainless steel cell (Harrick Scientific) fitted with 1.5 mm thick MgF_2 windows and an optical path length of 350 μm . The bleaching of sample molecules due to photo-induced decomposition was estimated to be smaller than 5% within 5 hours of laser operation — a typical time scale for continuous data collection. The sample cell is moved by computer controlled translational stages (Standa) in space after each measured spectrum to ensure that absorptions are not masked or enhanced due to sample burning onto the windows. Reference and signal IR beams are sent along a parallel path through a computer controlled spectrograph (Acton Research Corporation, SpectraPro-150) and detected by a 2x32 element MCT-array IR detector (InfraRed Associates, Inc.) and a high speed signal acquisition system and data acquisition software (Infrared

Systems Development Corp.) with a resolution of ca. 3 cm^{-1} . Collected signals are typically averaged over 1000 laser shots to account for shot-to-shot fluctuations of the laser. Differences in optical density (ΔOD) as small as 2×10^{-5} can be observed in the experiments after ca. 10-15 seconds of data collection.

C. Data Analysis Methods

Timescales for reactant and product evolution were determined by fitting the peak amplitude or peak area to a sum of exponentials using the Levenberg-Marquart method. Peak areas were determined by fitting spectra to a sum of Voigt functions and calculating the areas which were used to resolve the kinetics of overlapping absorption bands. This method will be referred to as the area fitting method. Peaks that are indistinguishable due to extensive overlap could not be fit to Voigt functions. In order to gain some insight into the dynamics of these heavily overlapped peaks, the infrared intensity at a single wavenumber was fit, and this method will be referred to hereafter as the trace fitting method. Note that the kinetics at a single wavenumber may be attributed to the dynamics of multiple peaks in close proximity and the timescales determined using this method may not be as accurate as those measured using the peak areas.¹⁸

D. Density functional theory calculations

Density functional theory (DFT) calculations have been used to assist in the characterization of the intermediate species and to facilitate an understanding of the dynamical behavior observed. The results from DFT calculations described here were carried out with Gaussian03¹⁹ using Becke's three-parameter exchange-correlation energy²⁰ combined with the Lee-Yang-Parr correlation functional,²¹ B3LYP.²² Generic basis sets used consisted of the LANL2DZ core potential²³ for ruthenium and 6-31G(d) (basis set A), and 6-31+G(d) (basis set B) basis sets for lighter atoms. Frequency calculations were carried out in order to ensure that configurations obtained correspond to minima on the potential energy surface. All calculated frequencies were scaled by a factor of 0.9614.²⁴ DFT calculations have been shown to be reliable in calculations of transition-metal complex structures, vibrational frequencies and energetics.²⁵

III. Results

A. Femtosecond UV pump/ IR probe spectroscopy of Ru₃(CO)₁₂

Data have been obtained on the photochemistry of Ru₃(CO)₁₂ in neat cyclohexane, a weakly coordinating solvent and neat THF, a Lewis base. All spectra are represented as infrared difference spectra in which a spectrum of the parent molecule before photoexcitation is subtracted from a spectrum of the photoexcited complex such that negative peaks represent parent molecules that have been depleted (hereafter referred to as the parent bleach) and positive peaks represent new species that have been formed at designated times after photoexcitation.

Cyclohexane results

Figure 2 contains the IR difference spectra for Ru₃(CO)₁₂ in cyclohexane after photoexcitation with 400-nm light (1.6 μJ). The large peaks between 1930 and 2100 cm⁻¹ represent the IR absorptions of the terminal carbonyls from all species formed. It is difficult to extract much useful information from this region as there are a multitude of carbonyl ligands from each photo-excited species that produce a spectrum of overlapping, indistinguishable peaks in solution.³ The kinetics of the peaks in this region were determined with the trace fitting method and respective time constants are reported in Table 1. In addition, three small peaks at 1815, 1833, and 1857 cm⁻¹ can be discerned and are shown in the inset of Figure 2. These peaks originate from bridged CO stretching frequencies which typically appear in the region between 1800 and 1900 cm⁻¹.^{3,10,13}

The dynamics of the largest bridging carbonyl peak centered at 1833 cm⁻¹ were determined with the area fitting method to have an exponential rise time of 23 ± 3 ps and a decay of 60 ± 5 ps, shown in Figure 3(a). Figure 3(b) shows the temporal evolution of the area of the peak centered at 1857 cm⁻¹. In nearly all experimental data, partial overlap of the terminal carbonyl band, centered at ca. 1935 cm⁻¹, with the 1857 cm⁻¹ band was observed. The decay of the terminal carbonyl band was taken into account in our tri-exponential fit of the 1857 cm⁻¹ peak by using a fixed decay time of 12 ps that represents the vibrational cooling of the neighboring terminal carbonyl band. The rise time of 134 ± 22 ps and a long slow decay of ca. 5 ns reflect the sole dynamics of the bridged carbonyl species. Due to the small signal,

the kinetics of the small peak at 1815 cm^{-1} were extremely difficult to obtain preventing further analysis.

IR difference spectra for $\text{Ru}_3(\text{CO})_{12}$ in cyclohexane excited with 266-nm light are similar to the 400-nm spectra (see Supporting Information S1). Kinetics of the transient species (Supporting Information S2) are reported in Table 1 and are similar to those measured for the photo-products of 400-nm excitation. In Figure 4 spectra after 266- and 400-nm excitations have been superimposed in order to illustrate their differences. The 400-nm excitation spectra in Figure 4 have been normalized according to the difference in size between the 266- and 400-nm bleach intensity. Bleach intensities can only provide an estimate of the relative quantum yield for reactant depletion at each excitation wavelength as product peaks overlap with the bleach, but comparing spectra using the bleach intensities appears is sufficient for a qualitative interpretation of the data. It is apparent from the figure that the peak at 1857 cm^{-1} is larger when 266-nm light was used to excite the cluster. In fact the 1857 cm^{-1} peak was ca. 70% larger when 266-nm light was used rather than 400-nm light, whereas the 1833 cm^{-1} peak was only ca. 18% larger when photoexcited with 266-nm light, relative to 400-nm excitation. As will be discussed later, the peak at 1833 cm^{-1} is assigned to the transient formed as a result of metal-metal bond cleavage and the peak at 1857 cm^{-1} to the transient formed upon CO dissociation.

THF results

IR difference spectra for $\text{Ru}_3(\text{CO})_{12}$ in THF photoexcited with 400-nm light are presented in Figure 5. The large peaks between 1930 and 2100 cm^{-1} represent the IR absorptions of the terminal carbonyls; their recovery times were measured using the trace fitting method and are reported in Table 2. Unlike the spectra collected in cyclohexane (Figure 2 inset), in THF there appears to be only one small peak at 1833 cm^{-1} (Figure 5 inset) that is assigned to a bridging carbonyl. This peak has a rise time of $8 \pm 2\text{ ps}$ and a decay of $53 \pm 9\text{ ps}$ and appears to shift to higher energy (i.e. blue shift) with a time constant of $124 \pm 12\text{ ps}$ (Figure 6). The shift in center frequency could be attributed to the process of vibrational cooling or might be indicative of growth of a second peak on the higher energy side of the peak at 1833

cm^{-1} . Data collected using 266 nm excitation (see Supporting Information S3) have a similar behavior to that observed after 400 nm excitation, however, dynamics were more difficult to capture as the peak amplitude was considerably smaller as a result of lower pump power.

B. DFT Results

Geometry optimizations and frequency calculations were performed for the starting material $\text{Ru}_3(\text{CO})_{12}$ and transient species. Figure 7a illustrates the optimized geometry for $\text{Ru}_3(\text{CO})_{12}$. Unlike the published crystal structure,⁵ these results show a low symmetry complex in which each metal and its four accompanying carbonyls are tilted by approximately 12-15 degrees off of the plane defined by the three metal atoms. It is likely that in order to increase the packing efficiency the cluster prefers a more symmetric geometry in the crystal, whereas it may tilt in the gas phase to minimize steric interactions. Generally the bond lengths and angles of the calculated gas phase cluster are quite similar to those of the experimentally measured crystal structure (see Table S1 in Supporting Information). Calculated frequencies and relative intensities for $\text{Ru}_3(\text{CO})_{12}$ (see Table S2 in Supporting Information) agree well with experimental results reported here and previously.³

The structures for the transient complexes discussed in our experimental work were calculated using DFT and provide the first calculated structures ever reported for these complexes. Solvated and unsolvated forms of the bridged carbonyl complexes are shown in Figures 7 and 8. The bridged carbonyl vibrational frequencies and corresponding amplitudes are listed in Table 3 and selected structural parameters are listed in Table 4. A complete list of the calculated vibrational frequencies can be found in the Supporting Information, Tables S2 and S3. Calculated thermodynamic stability of the complexes relative to the parent complex, $\text{Ru}_3(\text{CO})_{12}$, are listed in Table 5. Unsolvated forms of the transients were calculated using both basis set A and B and it was found that the structures were similar at both levels of theory, therefore only basis set A was used for the solvated complexes.

The structure for the metal-metal cleaved complex (**I**) is shown in Figure 7b. This structure was found by step-wise increases in the length of one Ru-Ru bond followed by geometry optimization at each step

to locate the energetic minimum. The optimized structure has a bridging CO spanning two metals that are still bonded (labeled Ru2 and Ru3 in Figure 7b). In contrast, all previous suggestions for the structure of complex **I** hypothesized that the CO would span the gap between the two metals with the broken bond so that the cluster could maintain an 18 electron count at each metal center.^{6-8,10,16} Although the structure for **I** does not maintain an even electron count on every metal, this new structure for **I** will be more susceptible to solvation at Ru1 thereby increasing its stability. The bond between Ru1 and Ru2 in complex **I** is lengthened with respect to the Ru1-Ru2 bond in the parents complex, and leads us to believe that if a strong π -acceptor solvent molecule were to bind to Ru1, the cluster could easily fragment into a solvated monomer and bridged CO dimer as was previously observed.¹⁰

Propane and THF solvated forms of **I** were calculated and are shown in Figures 7c and 7d, respectively. In all cases, the solvent molecule is coordinated to Ru1, the metal center that is lacking a bridged carbonyl. Attempts to calculate a solvated complex in which the solvent molecule is coordinated to Ru3 have failed, leading us to conclude that the best site for solvation is at the coordinatively unsaturated metal center Ru1. By comparing the metal to bridged CO distances for Ru2 and Ru3 (Ru3-C4 and Ru2-C4) it is evident that the bridging carbonyl is almost equidistance between the two metals with a small tendency towards Ru2 (see Table 4). It appears that the type of solvent has only a small effect on the local structure of the bridged carbonyl and the vibrational frequency (Table 3), probably because the site for solvation is two metals away from the bridged carbonyl. The calculated stabilities of the solvated complexes indicate that the THF solvated complex is more stable than the propane solvated form (Table 5). Correspondingly the metal-solvent distance decreases from propane to THF and is indicative of a stronger interaction with THF.

DFT calculations have been done for the two possible geometries for the CO-loss transients, an axial CO-loss and an equatorial CO-loss species (Figure 8). When an axial carbonyl was removed from the starting complex, $\text{Ru}_3(\text{CO})_{12}$, the bridging carbonyl complex, shown in Figure 8a, complex **II_{ax}**, was found to be the lowest energy structure. From the vibrational frequencies and the structure, it is clear that there is at least one bridged carbonyl spanning metals 1 and 3 (Table 4), labeled C4. Inspection of

the distances between Ru1-C4 and Ru3-C4 indicate that the bridge is asymmetric with bond lengths of 1.915 and 2.415 respectively. The bridged carbonyl vibrational frequency at 1884 cm⁻¹ (1862 cm⁻¹ with basis set B) corresponds to the stretch of only this carbonyl group. In addition, there is a terminal carbonyl with partial bridging character, labeled C5 in Figure 8a. The bridging for C5 is quite asymmetric with the stronger, shorter bond between C5 and Ru3. The vibrational frequency for this carbonyl group is 1954 cm⁻¹ which is higher than most bridged carbonyl frequencies. However, the carbonyl group labeled C5 is closer to the Ru1 metal center in complex **II_{ax}** as compared to the parent complex and the metal carbonyl angle for Ru3-C5-O5 of 168.4° is more bent than observed in the parent complex. In summary, there appears to be some interaction between this carbonyl (C5) and the metal center Ru1 although it is difficult to say if it could be considered a fully bridging carbonyl.

It is surprising that the coordinatively unsaturated metal center, Ru1, is donating one of its carbonyls (C4) to form the more significant bridge because this metal center is the coordinatively unsaturated metal. Inspection of the charge distribution among the three metal centers shows that Ru1 is considerably more positive than Ru2 and Ru3 and therefore the remaining metals do little to stabilize the coordinatively unsaturated metal center. Despite our efforts to locate another structure with a better distribution of charge among the three metal centers, complex **II_{ax}** is consistently the most stable carbonyl loss complex, indicating that stabilization must come from the bridging carbonyls. As noted earlier, the major bridging carbonyl, labeled C4, is asymmetrically bridged (with the Ru1-C4 bond being shorter) allowing some stabilization of the coordinatively unsaturated metal center Ru1. In addition, it is likely that the second weakly bridging carbonyl (C5) provides some added stability to Ru1.

In the case of the CO loss complex, it is first necessary to determine whether an axial or equatorial CO is dissociated. It was suggested by Bentsen et al. that an equatorial CO is initially photodissociated and that the complex rapidly isomerizes to an axially vacant structure at 110 K.³ We performed DFT calculations on an equatorially vacant cluster and found that the resulting structure lacks bridging carbonyls (Figure 8d, structure **II_{eq}**). The Ru3-C4 and Ru1-C5 distances for **II_{eq}** are substantially longer

than those observed for \mathbf{II}_{ax} . The Ru-C-O bond angles for \mathbf{II}_{eq} are quite similar to those observed for the parent molecule. Finally, the lowest carbonyl vibrational frequency at 1963 cm^{-1} consists of antisymmetric vibrations from the four axial carbonyls on Ru1 and Ru2, rather than a single carbonyl stretch as was observed for the major bridging carbonyl in \mathbf{II}_{ax} . This is consistent with Bentsen et al.'s observation that the \mathbf{II}_{eq} lacks bridging carbonyls.³

The axial vacant complex, \mathbf{II}_{ax} is more stable than the equatorially vacant complex, \mathbf{II}_{eq} , by 7.4 kcal mol^{-1} (Table 5); therefore isomerization of the complex to an axially vacant structure is thermodynamically favorable. The roles of each of these complexes in the context of the experimental results are discussed further in Section IV.

The solvated structures of complexes \mathbf{II}_{ax} and \mathbf{II}_{eq} were optimized with propane and THF using basis set A, and results are presented in Figure 8 and Tables 4-6. In the case of complex \mathbf{II}_{ax} , the input structure for the geometry optimization was the parent complex, $\text{Ru}_3(\text{CO})_{12}$, with a solvent molecule in place of one of the axial carbonyls. As can be seen in Figures 8b and 8c, both the propane and THF solvated complexes converged to structures containing a bridged carbonyl. Solvated forms of complex \mathbf{II}_{eq} are shown in Figures 8d-f and, as with the unsolvated form, the solvated \mathbf{II}_{eq} complexes contain no bridging carbonyls.

IV. Discussion

Photochemistry of $\text{Ru}_3(\text{CO})_{12}$ in non-coordinating solvents

In these experiments, the spectra measured for the bridging carbonyl region show unique features that have not been observed in any spectra reported previously.^{3,10,13} A detailed characterization of the photoproducts of $\text{Ru}_3(\text{CO})_{12}$ in cyclohexane is based on the kinetics of the bridging carbonyl peaks and a comparison of the intensities at each pump wavelength. Based on their kinetics, one can see that the 1833 cm^{-1} peak and the 1857 cm^{-1} peak are uncorrelated, and hence result from independent species.

The peak at 1857 cm^{-1} is assigned to the carbonyl-loss species, \mathbf{II}_{ax} . Figure 4 shows that this peak is more prominent when 266 nm light is used as the excitation wavelength. This assignment is based on

the fact that, in general, UV absorptions of metal carbonyls lead to CO dissociation^{3,10} and electronic absorption studies of $\text{Ru}_3(\text{CO})_{12}$ have assigned the UV band to a MLCT state that leads to CO dissociation.¹⁴ In addition, the quantum yields for photosubstitution products, which are generally believed to result from CO loss, were shown previously to increase significantly as the excitation wavelength was shortened which is consistent with our observations.^{7,8}

The dynamics of the 1857 cm^{-1} peak also support its assignment to complex II_{ax} . At both excitation wavelengths, 266 and 400 nm, this peak was observed to grow in with a time constant of 134-158 ps and remain constant out to 800 ps. It is expected that the bridged carbonyl complex will survive until it recombines with the dissociated CO (in non-coordinating solvents). The rate for CO/cluster recombination is limited by the rate of diffusion and the weak binding strength of the alkane and will occur in the time frame of μs .⁸

The peak at 1833 cm^{-1} is assigned to the metal-metal bond cleavage complex, **I**. The wavelength comparison study presented in Figure 4 shows that the intensity of the 1833 cm^{-1} peak is similar for both pump wavelengths. This is in agreement with previous studies in which the photofragmentation quantum yields (in coordinating solvents) were found to be wavelength independent.^{7,8,10} The dynamics of this peak are consistent with our assignment. The complex was observed to form quickly (15-23 ps) and decay quickly (60-63 ps). It is expected that the product of metal-metal cleavage is short lived because the two metals are hinged together by the third and cannot diffuse away resulting in fast recombination.

The small peak at 1815 cm^{-1} cannot be definitively assigned because of the low signal to noise. One can see from inspection of the spectra in Figure 2 that the small peak at 1815 cm^{-1} is long lived like its neighbor at 1857 cm^{-1} . This similarity in behavior leads us to believe that the 1815 cm^{-1} peak may be attributed to a CO loss complex. In this case, there may be another configuration for complex **II** that we are unable to locate using DFT.

The simultaneous observation of both **I** and II_{ax} was overlooked in previous studies due to limitations in time resolution or detection sensitivity. In the matrix studies by Bentsen et al. it was observed that

photofragmentation was blocked by the matrix.³ If complex **I** was formed in the matrix studies, it may have reformed the starting material before IR spectra could be collected.³ In the solution phase, flash photolysis study by Grevels et al. the instrument response time was 80 ns, exceeding the lifetime of complex **I** by three orders of magnitude.¹⁰ In the ultrafast Vis-pump IR-probe study by Vergeer et al. only complex **I** was observed to form.¹³ It is likely that complex **II_{ax}** was not observed in this study because the excitation intensity or the detection sensitivity were not sufficient; as can be seen in Figure 4, the peak at 1857 cm⁻¹ is barely discernable when a low pump power is used.²⁶ In Vergeer's study, the 1833 cm⁻¹ peak assigned to complex **I** was reported to have a rise time of 3.9 ± 0.9 ps in n-heptane solvents;¹³ this is faster than the rise times measured in our experiments. This disparity may be attributed to different methods for kinetic fitting as it is difficult to distinguish peaks at early times after photoexcitation because the broad and intense terminal carbonyl peaks are overlapping the bridged carbonyl absorption(s). The decay time we measured for the 1833 cm⁻¹ absorption (60-63 ps) is consistent with the decay time measured by Vergeer et al. (56.6 ± 6 ps), and this lends support to both of our assignments.

DFT calculations of **I** predict a bridged CO vibrational frequency of 1840 cm⁻¹ whereas **II_{ax}** has a calculated vibrational frequency of 1862 cm⁻¹ (basis set B, Table 3). This is consistent with the relative position of **I** and **II_{ax}** observed experimentally. In addition, DFT predicts that **I** exhibits a relative peak amplitude that is 2.1 times larger than **II_{ax}**.²⁷ It is difficult to draw direct comparisons of relative peak amplitudes from the experimental data since it is not known whether the quantum yields for **I** and **II_{ax}** are identical, however, in all experiments (at either 266 or 400 nm pump, and at a variety of pump powers) the peak for **I** is considerably larger than **II_{ax}**.

Our DFT studies are also consistent with Bentsen and Wrighton's work in which they demonstrated that a transient is formed from the photodissociation of an equatorial CO. They were only able to trap the equatorially vacant complex in a matrix of 2-MeTHF at 90 K and the complex did not contain bridged carbonyls.³ Similarly, the calculated structure for **II_{eq}** lacks bridging carbonyls. Bentsen and Wrighton identified **II_{eq}** at 90 K and observed that it rearranges to **II_{ax}** upon warming the matrix to 110

K.³ Our calculations indicate that \mathbf{II}_{ax} is considerably more stable than \mathbf{II}_{eq} , thus providing a thermodynamic driving force for this isomerization. It is likely that \mathbf{II}_{eq} is formed prior to \mathbf{II}_{ax} in our experiments, which explains why it takes an average of 139 ± 19 ps to form \mathbf{II}_{ax} ; however, no feature in our spectra can be positively attributed to \mathbf{II}_{eq} as it contains no bridging carbonyls, and the terminal carbonyl bands will overlap with those of the parent, complex **I**, and complex \mathbf{II}_{ax} .

There are a variety of theories that can be applied to this system in order to explain why both **I** and \mathbf{II}_{ax} form simultaneously at a single excitation wavelength. The first theory is that excitation of $\text{Ru}_3(\text{CO})_{12}$ populates both MLCT and $\sigma^* \leftarrow \sigma$ states directly. The MLCT (UV) band for $\text{Ru}_3(\text{CO})_{12}$ is considerably larger than the $\sigma^* \leftarrow \sigma$ (Vis.) band, therefore excitation of the cluster at 400 nm may directly populate the MLCT due to the overlap of the two bands. However, at 266 nm the tail of the absorption band for the $\sigma^* \leftarrow \sigma$ transition is expected to be extremely small and it is not likely that the wavelength independent quantum yield for the metal-metal bond cleavage channel results from overlapping UV and visible absorption bands. A second possibility, suggested by Desrosiers et al., is that after excitation with UV light the MLCT state associated with the CO loss channel is initially populated and the lower energy σ^* state associated with the metal-metal cleavage channel is subsequently populated via internal conversion.⁸ The process of internal conversion can be as fast as a few hundred femtoseconds²⁸ and this seems to be a reasonable explanation for the observation of two channels at short wavelengths. A third explanation is that excitation into the σ^* state and subsequent rearrangement of the molecular geometry results in an energetic lowering of the electronic states associated with the CO loss channel as was observed for $\text{Mn}_2(\text{CO})_{10}$.²⁹ Finally, the dipole forbidden transition predicted by Delley and coworkers to be energetically equal to the $\sigma^* \leftarrow \sigma$ transition may result in weakening of the metal carbonyl bond.¹⁵

Photochemistry of $\text{Ru}_3(\text{CO})_{12}$ in THF

The bridged carbonyl complex(es) observed in THF are the first ever reported under ambient conditions. Previous studies of the photo-induced dynamics of $\text{Ru}_3(\text{CO})_{12}$ in THF have shown that a

THF molecule solvates and stabilizes the photo-products but no study has conclusively demonstrated whether these complexes contain bridged carbonyls.^{3,8,9} This is important because understanding the nature of the photoproducts improves our understanding of the subsequent chemistry of these complexes.

In the spectra collected for $\text{Ru}_3(\text{CO})_{12}$ in THF it is not obvious whether there is one peak that shifts its position or two peaks with different dynamics. If the feature at 1820-1850 cm^{-1} is attributed to a single peak, the peak center shift to higher energy is a consequence of vibrational relaxation as the timescale is consistent with the timescale for vibrational relaxation of metal hexacarbonyl complexes in alkanes.³⁰ The dynamics of this peak (Table 2) and its position suggest that it results from a solvated form of species **I**. This assignment is consistent with a previous study in which 395 nm irradiation of $\text{Ru}_3(\text{CO})_{12}$ in THF produced a transient with a lifetime of 50 ms that was assigned to a THF stabilized form of **I**.⁸ In this scenario, complex **II_{eq}** is likely formed and solvated by THF consequently preventing the formation of the bridged CO complex **II_{ax}**.³

There is one major inconsistency with the assignment of the 1820-1850 cm^{-1} feature as one peak. The dynamics of the feature indicate that it grows in and decays with rates that are similar to those observed for complex **I** in cyclohexane. However, it does not decay back to the baseline, instead it maintains an amplitude of ca. 0.6 mOD out to 800 ps. There may be two modes of THF solvating the cluster, the first being oxygen solvation that traps complex **I** in its bridged form and the second being alkyl solvation resulting in some population that is able to recover to the starting material as was observed in cyclohexane. This hypothesis was tested by exploring the photo-induced solvation dynamics of $\text{Cr}(\text{CO})_6$ in THF.³¹ It was clear from these experiments that upon CO dissociation, the $\text{Cr}(\text{CO})_5$ fragment is solvated by the oxygen group on THF within the timescale of vibrational relaxation and no alkyl solvated form of $\text{Cr}(\text{CO})_5$ was detected. This result is not surprising since the distance from oxygen to the β -carbons is the same as the distance between the β -carbon and the oxygen in ethanol, a solvent which shows solvation at the hydroxyl group rather than the alkyl chain.³²

If the feature at 1820-1850 cm^{-1} is actually attributed to two peaks, then the absence of an isosbestic point suggests that the peaks result from unrelated species. Based on our DFT results and the dynamics of the feature, the large peak at 1833 cm^{-1} is attributed to complex **I** and the peak at ca. 1840 cm^{-1} is assigned to a THF solvated form of **II_{ax}**. The early time peak position and dynamics for the feature (8 ± 2 ps rise and 53 ± 9 ps decay) are extremely close to the average dynamics observed for **I** in cyclohexane (17 ± 2 ps rise and 61 ± 4 ps decay). At later times, relative position and long lived nature of the peak in THF are consistent with the position and dynamics of **II_{ax}** in cyclohexane. In this scenario, the center frequency shift (i.e. blue shift) of the feature of $\tau = 124$ ps is attributed to the formation time of the THF solvated **II_{ax}** and is within error of the average formation time of **II_{ax}** in cyclohexane (139 ± 19 ps). It seems possible that THF may be able to stabilize **II_{ax}** in a non-bridged form, but DFT results clearly indicate that the THF solvated structure contains bridged carbonyls. It is important to note that the DFT generated structure for THF solvated **II_{ax}** was found by starting the optimization from the parent complex with one of the axial CO's replaced with THF.

The two peak hypothesis and assignments are further supported by previous work. Matrix studies by Bentsen et al. indicate that a bridged carbonyl complex resulting from CO dissociation forms in a 2-MeTHF matrix, however, they were unable to say whether this complex was solvated by 2-MeTHF.³ While it has been suggested by Benson et al. that the bridged carbonyl complex they observed might be an unsolvated form of **II_{ax}**,³ our DFT results clearly indicate that a THF solvated form of the complex is thermodynamically more favorable (see Table 5). In summary, if the feature between 1820 and 1850 cm^{-1} results from two peaks, the peaks at 1833 cm^{-1} and 1840 cm^{-1} are assigned to the THF solvated forms of **I** and **II_{ax}**, respectively, based on our cyclohexane and DFT results and previous work. However, an irrefutable assignment of this feature requires better wavenumber resolution in order to determine whether it results from one or two peaks.

V. Conclusions

The dynamics of $\text{Ru}_3(\text{CO})_{12}$ after photo-excitation was followed by monitoring the small but distinct infrared absorptions of the bridging carbonyls. The results of these studies are summarized Figure 9. In both cyclohexane and THF, excitation of $\text{Ru}_3(\text{CO})_{12}$ with either 266- or 400-nm light results in formation of two photoproducts, the first is a metal-metal cleavage complex (**I**, left side of Figure 9) and the second is a carbonyl loss product (**II**, right side of Figure 9). Complex **I** showed an average formation time of 17 ± 1 ps and an average lifetime of 61 ± 4 ps in cyclohexane. The formation rate for **I** may be correlated with the rate for fast vibrational cooling observed in the terminal carbonyl bands (10-30 ps).

Based on our DFT and experimental results as well as previously published results,³ it is likely that an equatorially CO is dissociated resulting in formation of **II_{eq}** that isomerizes to **II_{ax}**. The DFT studies have demonstrated that the equatorially vacant cluster (**II_{eq}**) is unstable relative to its axially vacant isomer (**II_{ax}**) and contains no bridging carbonyls. Therefore, the bridging carbonyl observed in the experiments can only result from an axially vacant complex. The average formation time for **II_{ax}** of 139 ± 19 ps in non-coordinating solvents is likely to involve isomerization from an equatorially vacant to an axially vacant species and subsequent or concomitant bridging of a CO. The lifetime of **II_{ax}** is greater than the timescale of our experiment and has been demonstrated by others to depend on the concentration of CO with a rate of decay that is diffusion limited.⁹

In THF, it is impossible to definitively state whether there is one or two bridging carbonyl absorptions, however, because the feature at $1830\text{-}1850\text{ cm}^{-1}$ exhibits early time dynamics but does not decay to the baseline, it seems more likely that there are two peaks. In which case, the peaks are likely to result from THF solvated forms of **I** and **II_{ax}**. This assignment is supported by our cyclohexane spectra, DFT studies and previous work.^{3,8} It is interesting that in THF, **II_{ax}** forms with a rate that is similar to the formation rate in cyclohexane; if **II_{eq}** is solvated and stabilized by THF one might expect it to be longer lived and slow the formation of **II_{ax}**. Therefore, it is likely that **II_{ax}** formation is also correlated with vibrational cooling as a vibrationally hot form of **II_{eq}** will have sufficient thermal energy to dissociate the solvated THF molecule.

One of the main objectives in our studies was to find out how many bridged carbonyl complexes are formed after UV or visible light excitation of $\text{Ru}_3(\text{CO})_{12}$. Prior to the results presented in this paper no study had ever characterized more than one bridged carbonyl complex^{3,10,13} despite the indirect evidence that there must be two forming simultaneously (based on the simultaneously formation of both photofragmentation and photosubstitution products).^{7,8,16} Consequently, Grevels and co-workers¹⁰ suggested that the path to photofragmentation after UV excitation of the cluster involved formation of only one bridged carbonyl complex, II_{ax} , which subsequently underwent photofragmentation. Our studies have resolved that there are two bridged carbonyl complexes formed after excitation at a single wavelength and the hypothesis that multiple bond cleavage channels are accessed producing multiple photoproducts^{7,8} is supported. Our results indicate that Grevel et al.'s favored mechanism for fragmentation after short wavelength excitation is incorrect.¹⁰

Another objective of our studies was to determine the role of the bridged carbonyl complexes in coordinating solvents. THF was chosen because it was shown to block photofragmentation without changing photosubstitution yields.⁶⁻⁸ Based on our results it seems most likely that both bridged carbonyl complexes are formed after 400 nm excitation in THF and generally show similar behavior as was observed in cyclohexane. In our studies, complex **I** was extremely short lived in both THF and cyclohexane (53 – 63 ps). In cyclohexane we presume that **I** decays back to the starting complex because longer time studies were never able to characterize a metal-metal cleavage transient in alkane solvents.⁸ However, in THF a second transient must be formed that is stabilized by THF and lacks bridging carbonyls because flash photolysis studies have located a transient formed from long wavelength irradiation in THF that is absent in alkane solvents.⁸ We are currently investigating the nature of the second THF stabilized transient as well as the role of the bridged carbonyl complex in π -backbonding solvents.

In summary, our combined experimental and theoretical studies provide additional insights into the photochemistry of $\text{Ru}_3(\text{CO})_{12}$ complexes and the nature and role of bridged carbonyl intermediates.

Acknowledgments

The National Science Foundation for funding, and the Office of Basic Energy Sciences, Chemical Sciences Division, of the U.S. Department of Energy under contract DE-AC02-05CH11231 for the use of some specialized equipment. M.F.K. acknowledges support by the Alexander von Humboldt foundation through a Feodor-Lynen Fellowship.

Supporting Information Available Containing spectra and kinetics of Ru₃(CO)₁₂ excited with 266 nm light in cyclohexane and THF; a plot of power dependent peak amplitudes for the bridged carbonyl peaks; DFT calculated structural parameters of the parent Ru₃(CO)₁₂; and all vibrational frequencies for the parent Ru₃(CO)₁₂, and complexes **I**, **II_{ax}**, and **II_{eq}**. This material is available free of charge via the Internet at <http://pubs.acs.org>.

REFERENCES

- (1) (a) Richmond, M.G. *Coord. Chem. Rev.* **2004**, *248*, 881. (b) Dyson, P.J.; McIndoe, S.J. *Transition Metal Carbonyl Cluster Chemistry*; Gordon and Breach Science Publishers: Amsterdam, Netherlands, 2000. (c) Michelin Lausarot, P.; Vaglio, G.A.; Valle, M. *J. Organomet. Chem.* **1984**, *275*, 233. (d) Kakiuchi, F.; Matsumoto, M.; Tsuchiya, K.; Igi, K.; Hayamizu, T.; Chatani, N.; Murai, S. *J. Organomet. Chem.* **2003**, *686*, 134. (e) Meijer, R.H.; Ligthart, G.B.W.L.; Meuldijk, J.; Vekemans, J.A.J.M.; L.A., H.; Mills, A.M.; Kooijman, H.; Spek, A.L. *Tetrahedron* **2004**, *60*, 1065. (f) Leadbeater, N.E. *J. Chem. Soc. Dalton. Trans.* **1995**, *18*, 2923. (g) Edwards, A.J.; Leadbeater, N.E.; Lewis, J.; Raithby, P.R. *J. Organomet. Chem.* **1995**, *503*, 15.
- (2) Wu, Y.M.; Bentsen, J.G.; Brinkley, C.G.; Wrighton, M.S. *Inorg. Chem.* **1987**, *26*, 530.
- (3) Bentsen, J.G.; Wrighton, M.S. *J. Am. Chem. Soc.* **1987**, *109*, 4530.
- (4) Bentsen, J.G.; Wrighton, M.S. *J. Am. Chem. Soc.* **1987**, *109*, 4518.
- (5) Churchill, M.R.; Hollander, F.J.; Hustchinson, J.P. *Inorg. Chem.* **1977**, *16*, 2655.

- (6) Desrosiers, M.F.; Ford, P.C. *Organomet.* **1982**, *1*, 1715.
- (7) Desrosiers, M.F.; Wink, D.A.; Ford, P.C. *Inorg. Chem.* **1985**, *24*, 1.
- (8) Desrosiers, M.F.; Wink, D.; Trautman, R.; Friedman, A.E.; Ford, P.C. *J. Am. Chem. Soc.* **1986**, *108*, 1917.
- (9) Dibenedetto, J.A.; Ryba, D.W.; Ford, P.C. *Inorg. Chem.* **1989**, *28*, 3503
- (10) Grevels, F.W.; Klotzbucher, W.E.; Schrickel, J.; Schaffner, K. *J. Am. Chem. Soc.* **1994**, *116*, 6229.
- (11) Hunstock, E.; Mealli, C.; Calhorda, M.J.; Reinhold, J. *Inorg. Chem* **1999**, *38*, 5053.
- (12) Johnson, B.F.G.; Lewis, J.; Twigg, M.V. *J. Organomet. Chem.* **1974**, *67*, C75.
- (13) Vergeer, F.W.; Hartl, F.; Matousek, P.; Stufkens, D.; Towrie, M. *Chem. Comm.* **2002**, 1220.
- (14) Tyler, D.R.; Levenson, R.A.; Gray, H.B. *J. Am. Chem. Soc.* **1978**, *100*, 7888.
- (15) Delley, B.; MAnning, M.C.; Ellis, D.E.; Berkowitz, J.; W.C., T. *Inorg. Chem.* **1982**, *21*, 2247.
- (16) Malito, J.; Markiewicz, S.; Poe, A. *Inorg. Chem.* **1982**, *21*, 4335
- (17) Shanoski, J.E.; Payne, C.K.; Kling, M.F.; Glascoe, E.A.; Harris, C.B. *Organomet.* **2005**, *24*, 1852.
- (18) All errors presented reflect 95% confidence intervals. In the case of the area fitting method, the errors presented do not take into account the goodness of fit of the Voigt function to the raw data.
- (19) Frisch, M.J.e.a. *Gaussian 03, Revision C.02*; Gaussian, Inc.: Wallingford, CT 2004
- (20) Becke, A.D. *J. Chem. Phys* **1993**, *98*, 5648.
- (21) Lee, C.; Yang, W.; Parr, R.G. *Phys. Rev. B.* **1988**, *37*, 785.

- (22) Stephens, P.J.; Devlin, G.J.; Chabalowski, C.F.; Frisch, M.M. *J. Phys. Chem.* **1994**, *98*, 11623.
- (23) Hay, P.J.; Wadt, W.R. *J. Chem. Phys.* **1985**, *82*, 299.
- (24) Scott, A.P.; Radom, L. *J. Phys. Chem.* **1996**, *100*, 16502.
- (25) Niu, S.; Hall, M.B. *Chem. Rev.* **2000**, *100*, 353.
- (26) A linear dependence on excitation energy at 400 nm in our experiments confirmed that these peaks result from single photon processes (see supporting information figure S4).
- (27) In determining the relative amplitude of **I** vs. **II_{ax}**, all the vibrational frequencies for each molecule were internally scaled relative to the strongest vibrational mode in each molecule and then the relative amplitude of the two molecule were compared using these scaled amplitudes. The vibrational frequencies of these two molecules were also compared by scaling both to the largest vibrational mode of the parent molecule and the relative amplitude of **I** vs. **II_{ax}** using this method was 2.9:1.
- (28) Vlcek, A.J. *Coord. Chem. Rev.* **2000**, *200-202*, 933.
- (29) Baerends, E.J.; Rosa, A. *Coord. Chem. Rev.* **1998**, *177*, 97.
- (30) Dougherty, T.P.; Heilweil, E.J. *Chem. Phys. Lett.* **1994**, *227*, 19.
- (31) Unpublished Data
- (32) Kling, M.F.; Glascoe, E.A.; Shanoski, J.E.; Payne, C.K.; Mork, B.V.; Tilley, T.D.; Harris, C.B. *Organomet.* **2005**, *In Preparation*, . Shanoski, J.; Glascoe, E.; Harris, C.B. *J. Phys. Chem. B* **2005**, *In Preparation*.
- (33) The first 50 ps were removed because an early time low-energy shift of the peak made the longer time high-energy shift difficult to determine. The low-energy shift may result from difficulty fitting the peak at early times because it is vibrationally excited, very broad and rather weak in amplitude.

Table 1. Exponential fitting parameters of product and bleach recovery peaks from Ru₃(CO)₁₂ in cyclohexane excited with 266 or 400 nm light.

<i>Product Peaks in Cyclohexane</i>				
Peak /cm ⁻¹	$\tau_{400\text{nm}}/\text{ps}$		$\tau_{266\text{nm}}/\text{ps}$	
1833	23 ± 3	rise	15 ± 2	rise
	60 ± 5	decay	63 ± 5	decay
1857	134 ± 22	rise	158 ± 42	rise
	ns	decay	ns	decay
1935	12 ± 1	decay	22 ± 4	decay
	128 ± 24	decay	206 ± 72	decay
1950	7.8 ± 0.3	decay	8 ± 1	decay
	101 ± 1	decay	67 ± 9	decay
1999	13 ± 1	decay	26 ± 2	decay
	137 ± 2	decay	152 ± 6	decay
2018	97 ± 1	decay	6 ± 1	rise
			94 ± 1	decay
2039	17 ± 1	decay	22 ± 1	rise
			291 ± 26	decay
2049	2 ± 2	rise	6.3 ± 0.2	decay
	88 ± 1	decay	83.2 ± 04	decay
2092	262 ± 10	decay	27 ± 16	decay
			170 ± 29	decay
2104	325 ± 9	decay	201 ± 8	decay
<i>Bleach Peaks in Cyclohexane</i>				
Peak /cm ⁻¹	$\tau_{400\text{nm}}/\text{ps}$		$\tau_{266\text{nm}}/\text{ps}$	
2029	108.5 ± 0.2	rise	6 ± 1	decay
			58 ± 1	rise
2060	13 ± 1	rise	37 ± 1	rise
	68 ± 3	rise	164 ± 17	rise

Table 2. Kinetics of product and bleach recovery peaks from Ru₃(CO)₁₂ in THF excited with 266- or 400-nm light.

<i>Product Peaks in THF</i>				
Peak /cm ⁻¹	$\tau_{400\text{nm}}/\text{ps}$		$\tau_{266\text{nm}}/\text{ps}^a$	
1833	8 ± 2	rise		
	53 ± 9	decay		
1890	9 ± 2	decay		
	155 ± 29	decay		
1984	15 ± 2	decay	42 ± 9	decay
	98 ± 6	decay		
1991	17 ± 2	decay	8 ± 5	decay
	98 ± 5	decay	76 ± 15	decay
2016	93 ± 4	decay	110 ± 9	decay
2048	71 ± 1	decay	8 ± 1	decay
			104 ± 5	decay
<i>Bleach Peaks in THF</i>				
Peak /cm ⁻¹	$\tau_{400\text{nm}}/\text{ps}$		$\tau_{266\text{nm}}/\text{ps}$	
2031	9 ± 1	decay	6 ± 2	decay
	101 ± 1	rise	82 ± 5	rise
2063	25 ± 1	rise	87 ± 3	rise
	101 ± 3	rise		

^a Signal to noise was not sufficient to resolve kinetics for the bridged carbonyl peak at 1833 cm⁻¹ or the terminal carbonyl at 1890 cm⁻¹ after 266 nm excitation.

Table 3. Vibrational frequencies (cm⁻¹) and relative amplitudes for the bridged carbonyl group in the unsolvated and solvated forms of complexes **I** and **II_{ax}**.

	I	II_{ax} ^a
Unsolvated <i>Basis Set B</i>	1840 (0.39)	1862 (0.18)
Unsolvated ^b	1859 (0.34)	1884 (0.18)
Propane Solv.	1847 (0.27)	1879 (0.21)
THF Solv. ^c	1838 (0.19)	1886 (0.16)

^a Complex **II_{eq}** was found to have no bridging carbonyls. ^b Unless otherwise specified, basis set A was used for all calculations. ^c THF solvated complexes are solvated by the oxygen atom of the THF molecule.

Table 4. Calculated structural parameters of the parent molecule, Ru₃(CO)₁₂, as well as solvated and unsolvated forms of the transient complexes **I**, **II_{ax}**, and **II_{eq}**.

Complex ^a And Solvent	Distance (Å)								Angles (deg)			
	Ru1 -C4	Ru3 -C4	Ru1 -C5	Ru3 -C5	Ru1 - Ru3	Ru1 - Ru2	Ru2 - Ru3	Ru1- Solv. ^b	Ru1 -C4- Ru3	Ru1 -C5- Ru3	Ru1 -C4- O4	Ru3 -C5- O5
Parent	1.969	3.199	3.203	1.970	2.925	2.925	2.923	NA	63.8	63.7	173.1	173.0
II_{ax}	1.915	2.415	2.489	1.984	2.854	2.822	2.946	NA	81.6	78.4	150.3	168.4
II_{ax}..Propane	1.918	2.397	2.528	1.984	2.866	2.820	2.948	2.938	82.4	77.8	150.0	168.3
II_{ax}..THF	1.910	2.488	2.527	1.980	2.914	2.879	2.922	2.468	81.9	79.5	154.5	161.9
II_{eq}	1.945	3.230	3.160	1.976	2.843	2.938	2.897	NA	60.8	62.3	174.8	175.1
II_{eq}..Propane	1.949	3.255	3.190	1.974	2.845	2.940	2.915	2.216	60.2	61.6	174.5	174.3
II_{eq}..THF	1.953	3.307	3.226	1.971	2.855	2.950	2.928	2.350	59.3	61.1	174.2	174.1
	Ru3 -C4	Ru2 -C4			Ru1 - Ru3	Ru1 - Ru2	Ru2 - Ru3	Ru1 - Solv.	Ru3 -C4- Ru2			
I	2.205	2.054			4.980	3.190	2.918	NA	86.4			
I..Propane	2.212	2.043			4.960	3.232	2.946	2.691	87.5			
I..THF	2.219	2.042			4.981	3.226	2.979	2.431	88.6			

^a Atom numbers correspond to labels in Figures 7 and 8. ^b In the case of propane, the Ru1-solvent distances are measured from the metal to the hydrogen. For THF, the Ru1-solvent distance is measured from the oxygen.

Table 5. Stability of calculated complexes relative to the parent structure, Ru₃(CO)₁₂; smaller values indicate a more stable complex.

Complex and Solvent	ΔH° Basis Set A^a	ΔH° Basis Set B^b
I	23.8	23.9
I...Propane	24.2	24.9
I...THF	19.5	19.2
II_{ax}	26.5	23.8
II_{ax}...Propane	26.3	
II_{ax}...THF	19.7	
II_{eq}	33.9	31.2
II_{eq}...Propane	31.2	
II_{eq}...THF	22.5	

^a All enthalpies are reported in kcal mol⁻¹ and calculated at 298 K. ^b Standard enthalpies calculated from basis set A and B are similar and only a few calculations at the higher basis set were performed to illustrate this point.

Figure 1. Summary of the solvent and wavelength dependent photochemistry of $\text{Ru}_3\text{CO}_{12}$ clusters as it is currently understood. See text for details and references.

Figure 2. $\text{Ru}_3(\text{CO})_{12}$ in cyclohexane excited with 400 nm light (1.6 μJ). Spectra in the inset are fits overlaid on the raw data. Arrows indicate changes with increasing delay time.

Figure 3. Kinetics of $\text{Ru}_3(\text{CO})_{12}$ in cyclohexane excited with 400-nm light. (a) shows the 1833 cm^{-1} peak areas and the bi-exponential fit. (b) 1857 cm^{-1} peak area and corresponding fit.

Figure 4. Comparison of spectra when $\text{Ru}_3(\text{CO})_{12}$ is excited with 266-nm (blue/dashed) and 400-nm light (red/solid) in cyclohexane. The 400-nm spectra were normalized to the relative intensity of the 266-nm spectra based on a comparison of the 2060 cm^{-1} bleach for both excitation wavelengths.

Figure 5. Difference spectra of $\text{Ru}_3(\text{CO})_{12}$ excited with 400 nm (0.75 μJ) in a neat solution of THF. Spectra in the inset are fits overlaid on the raw data. Arrows indicates changes with increasing delay time.

Figure 6. (a) Kinetics of the bridged carbonyl complex of $\text{Ru}_3(\text{CO})_{12}$ excited with 400-nm light in THF. Data points correspond to peak area at each time. (b) Center frequency of the same peak and corresponding mono-exponential fit.³³

Figure 7. DFT optimized structures using basis set A. Lighter colored atoms are meant to provide a sense of depth and are behind the darker colored atoms. (a) $\text{Ru}_3(\text{CO})_{12}$ prior to excitation, (b) $\text{Ru}_3(\text{CO})_{12}$ with one metal-metal bond cleaved (**I**), and complex **I** solvated with (c) propane and (d) THF.

Figure 8. DFT optimized structures for the CO loss complex. (a) Unsolvated Complex **II_{ax}**, $\text{Ru}_3(\text{CO})_{10}(\mu\text{-CO})$ formed from axially CO dissociation and solvated with (b) propane and (c) THF. (d) unsolvated complex **II_{eq}**, $\text{Ru}_3(\text{CO})_{11}$ formed from equatorial CO loss and forms of **II_{eq}** solvated with (e) propane and (f) THF.

Figure 9. Principle species formed in irradiation of $\text{Ru}_3(\text{CO})_{12}$ in cyclohexane and THF. In order to visualize both reaction channels, the metal-metal cleavage channel is on the left side whereas the CO loss channel is on the right. The CO loss quantum yield is greater when the cluster is irradiated with 266 nm vs. 400 nm, while metal-metal cleavage quantum yields are similar after both 266 and 400 nm irradiation. See text for details. Energetics of all species were derived from DFT calculations using basis set A.

Figure 1. Glascoe, E.A.; Kling, M.F.; Shanoski, J.E.; Harris, C.B. “The Nature and Role of Bridged Carbonyl Intermediates in the Ultrafast Photo-induced Rearrangement of $\text{Ru}_3(\text{CO})_{12}$ ”

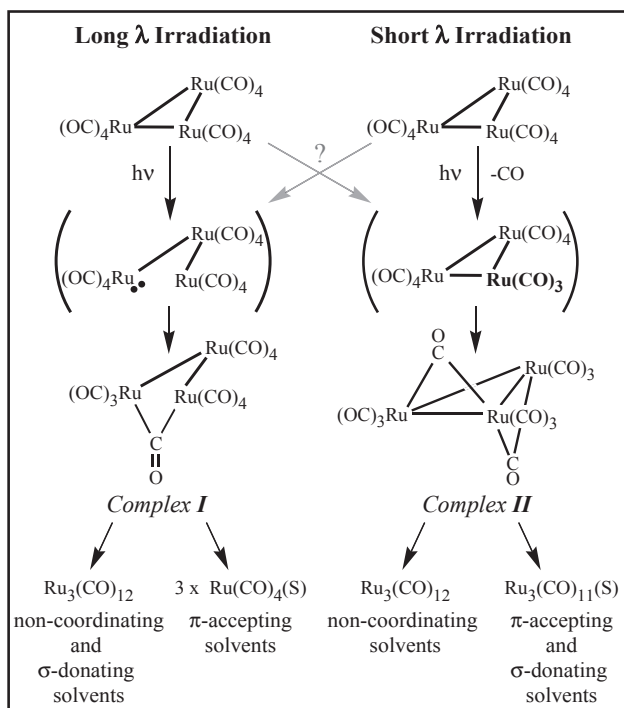


Figure 2. Glascoe, E.A.; Kling, M.F.; Shanoski, J.E.; Harris, C.B. “The Nature and Role of Bridged Carbonyl Intermediates in the Ultrafast Photo-induced Rearrangement of $\text{Ru}_3(\text{CO})_{12}$ ”

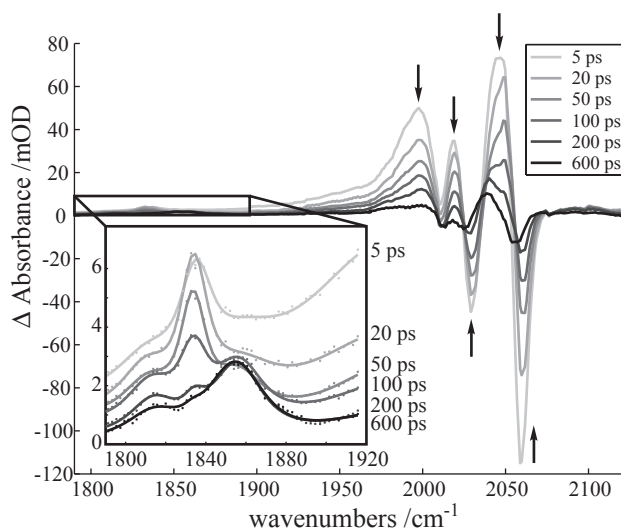


Figure 3. Glascoe, E.A.; Kling, M.F.; Shanoski, J.E.; Harris, C.B. “The Nature and Role of Bridged Carbonyl Intermediates in the Ultrafast Photo-induced Rearrangement of $\text{Ru}_3(\text{CO})_{12}$ ”

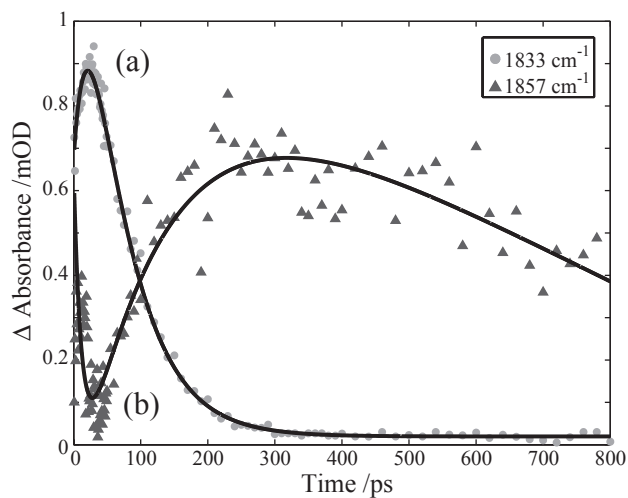


Figure 4. Glascoe, E.A.; Kling, M.F.; Shanoski, J.E.; Harris, C.B. “The Nature and Role of Bridged Carbonyl Intermediates in the Ultrafast Photo-induced Rearrangement of $\text{Ru}_3(\text{CO})_{12}$ ”

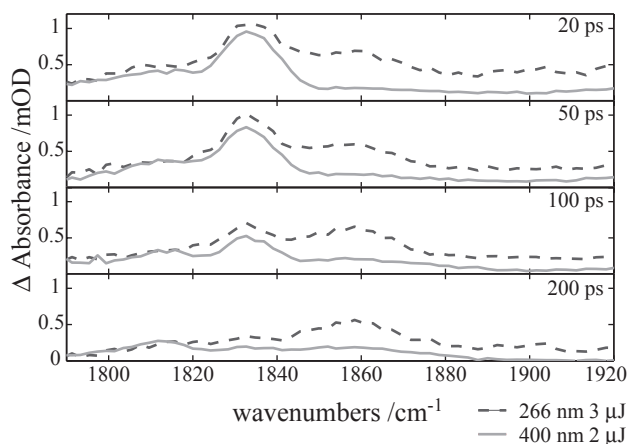


Figure 5. Glascoe, E.A.; Kling, M.F.; Shanoski, J.E.; Harris, C.B. “The Nature and Role of Bridged Carbonyl Intermediates in the Ultrafast Photo-induced Rearrangement of $\text{Ru}_3(\text{CO})_{12}$ ”

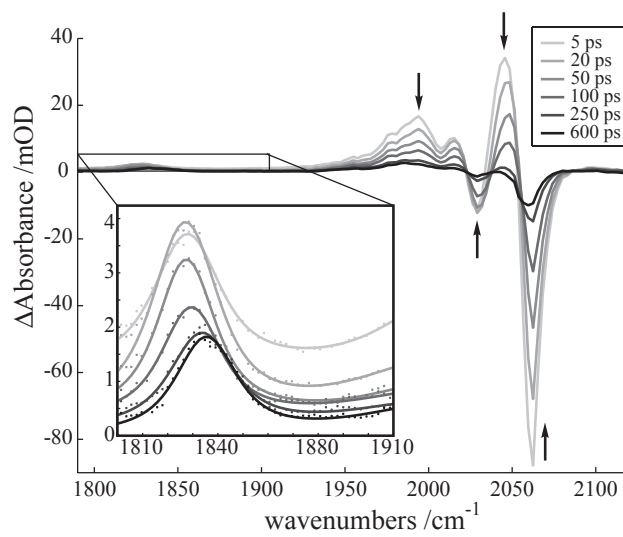


Figure 6. Glascoe, E.A.; Kling, M.F.; Shanoski, J.E.; Harris, C.B. “The Nature and Role of Bridged Carbonyl Intermediates in the Ultrafast Photo-induced Rearrangement of $\text{Ru}_3(\text{CO})_{12}$ ”

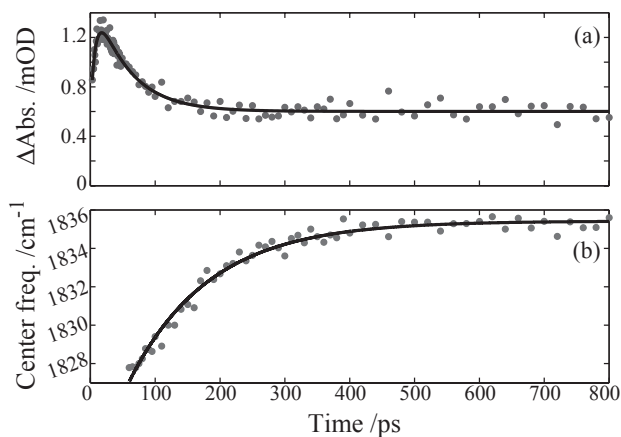


Figure 7. Glascoe, E.A.; Kling, M.F.; Shanoski, J.E.; Harris, C.B. “The Nature and Role of Bridged Carbonyl Intermediates in the Ultrafast Photo-induced Rearrangement of $\text{Ru}_3(\text{CO})_{12}$ ”

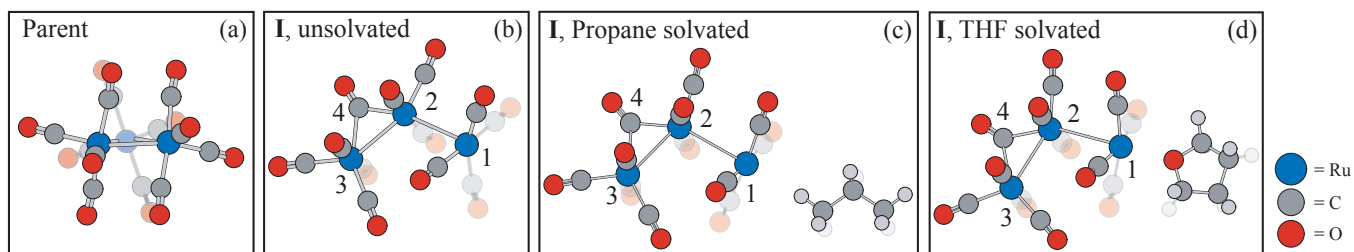


Figure 8. Glascoe, E.A.; Kling, M.F.; Shanoski, J.E.; Harris, C.B. “The Nature and Role of Bridged Carbonyl Intermediates in the Ultrafast Photo-induced Rearrangement of $\text{Ru}_3(\text{CO})_{12}$ ”

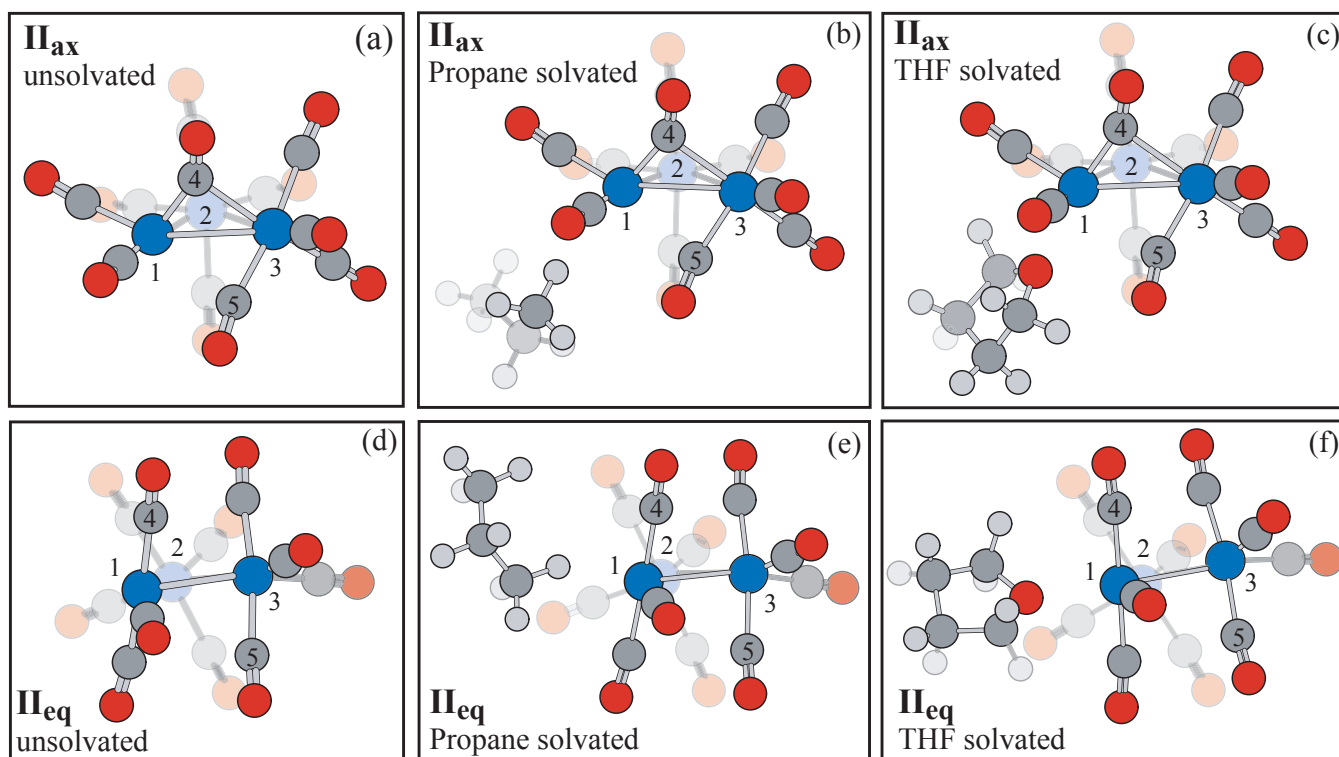
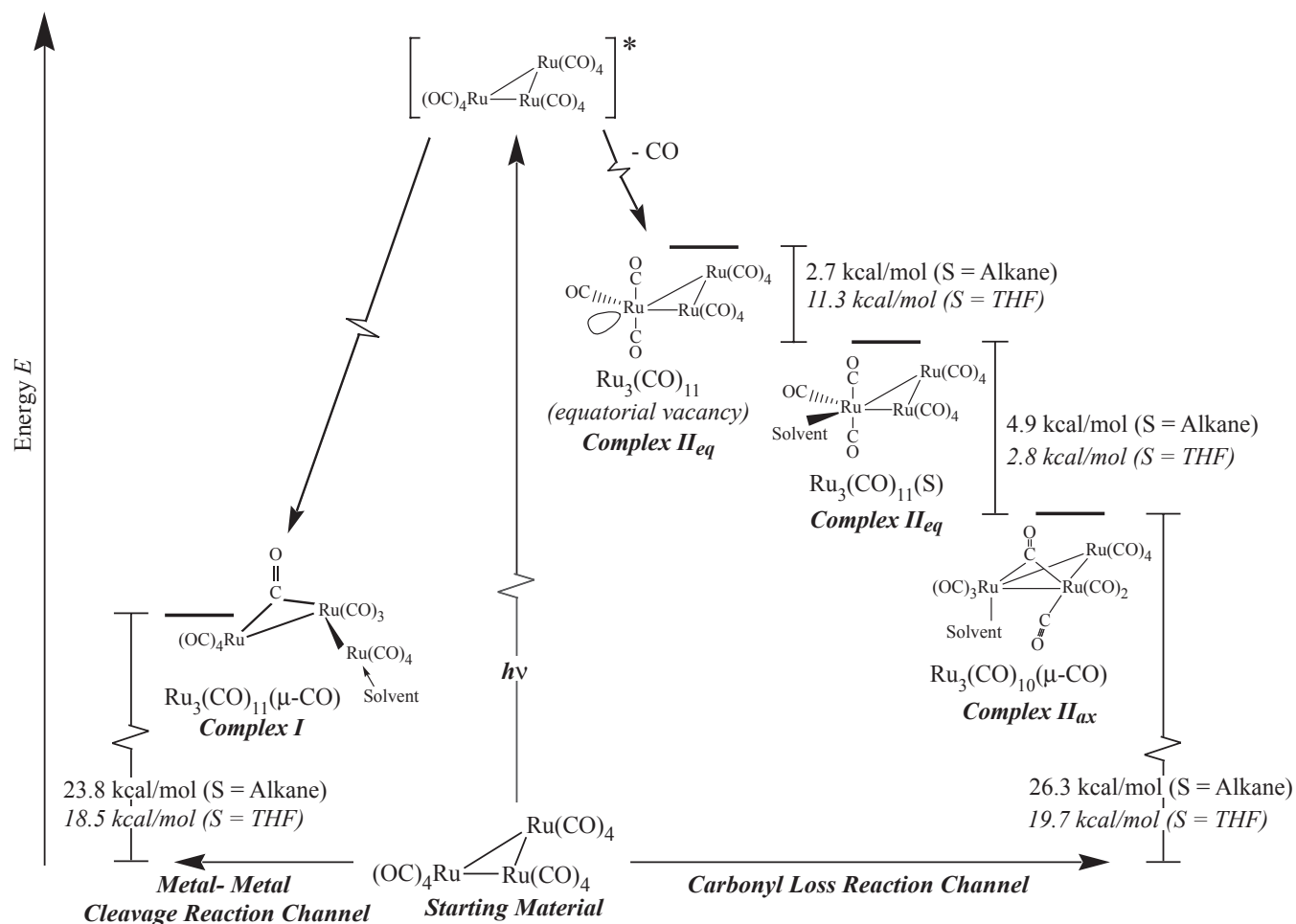


Figure 9. Glascoe, E.A.; Kling, M.F.; Shanoski, J.E.; Harris, C.B. “The Nature and Role of Bridged Carbonyl Intermediates in the Ultrafast Photo-induced Rearrangement of $\text{Ru}_3(\text{CO})_{12}$ ”



The Nature and Role of Bridged Carbonyl Intermediates
in the Ultrafast Photo-induced Rearrangement of
 $\text{Ru}_3(\text{CO})_{12}$

Elizabeth A. Glascoe, Matthias F. Kling,[‡] Jennifer E. Shanoski, and Charles B. Harris^{*}

*Contribution from the Department of Chemistry, University of California, Berkeley, California 94720,
and Chemical Sciences Division, Lawrence Berkeley National Laboratory, Berkeley, California 94720*

^{*} E-mail: cbharris@berkeley.edu

[‡] Present address: FOM Institute for Atomic and Molecular Physics (AMOLF), Kruislaan 407, 1098 SJ Amsterdam, The Netherlands.

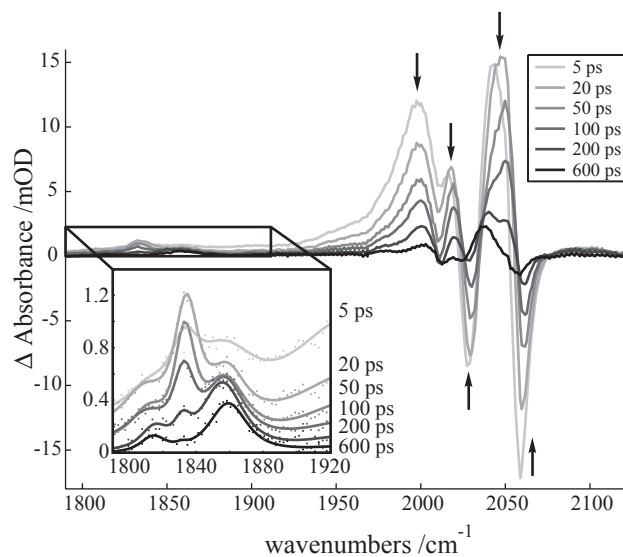


Figure S1. $\text{Ru}_3(\text{CO})_{12}$ in Cyclohexane excited with 266 nm light ($0.3 \mu\text{J}$). Arrows indicate changes with increasing delay time.

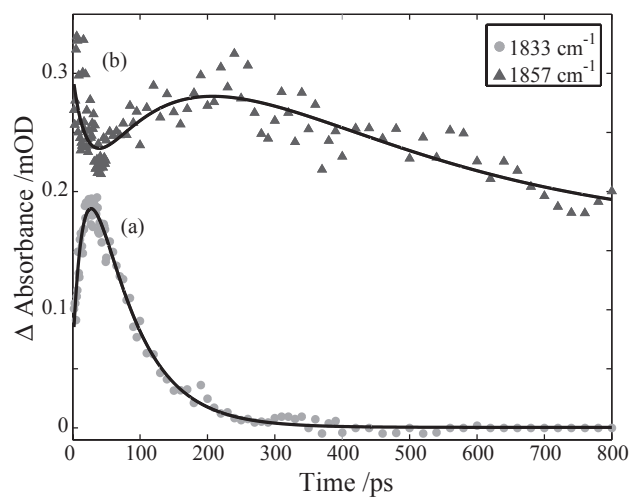


Figure S2. Kinetics of $\text{Ru}_3(\text{CO})_{12}$ in cyclohexane excited with 266 nm: (a) 1833 cm^{-1} peak areas (dots) together with a bi-exponential fit, (b) 1857 cm^{-1} peak areas (triangles) together with the corresponding fit; the data at 1857 cm^{-1} was raised vertically to allow an easy visualization of the data taken at 1833 cm^{-1} .

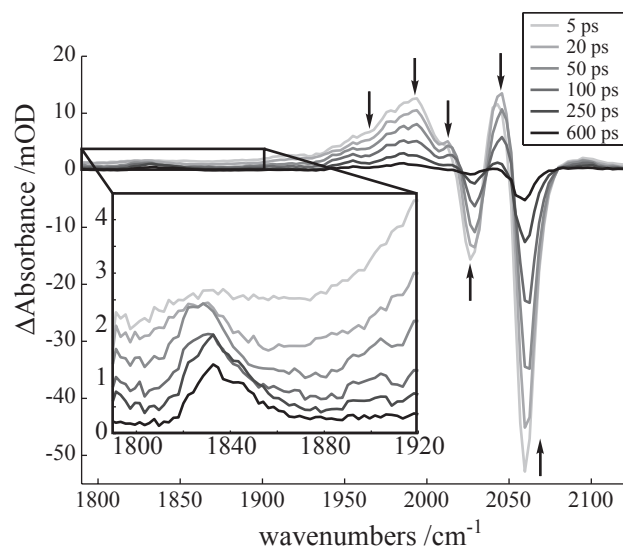


Figure S3. Difference spectra of Ru₃(CO)₁₂ excited with 266 nm (0.3 μ J) in a neat solution of THF.

Arrows indicate changes with increasing delay time.

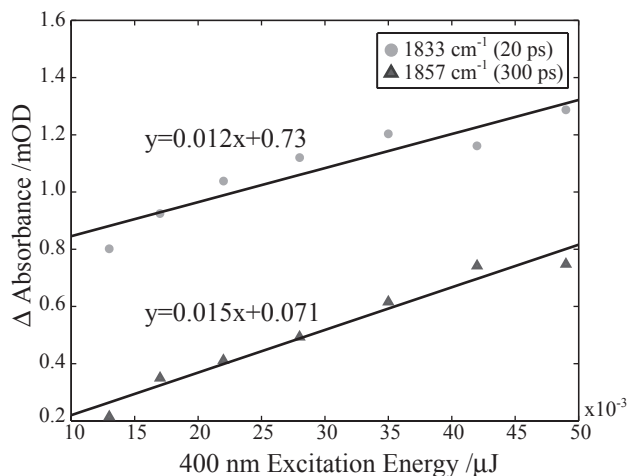


Figure S4. Power dependent peak amplitudes after photo-exciting $\text{Ru}_3(\text{CO})_{12}$ in cyclohexane with various energies of 400-nm light. The linear dependence of peak amplitude on excitation energy indicates that both peaks result from single photon processes. The energy was measured after a 400/800 nm beam splitter in order to maximize measurement accuracy, subsequently the beam passes through a series of optics prior to impinging on the sample. Therefore, the energy measurements reflect relative pump energies and not the actual energies of the 400-nm pulses used to photo-excite the sample. Because the peaks appear at different times it was necessary to measure the 1833 cm^{-1} peak at 20 ps and the 1857 cm^{-1} peak at 300 ps.

Table S1. Geometry optimized bond lengths and angles for the parent molecule Ru₃(CO)₁₂ prior to excitation.

Distance (Å)	Basis Set A^a	Basis Set B^a	exptl^b
Ru-Ru	2.924	2.929	2.854
Ru-C _{ax}	1.969	1.971	1.942
Ru...O _{ax}	3.115	3.116	3.071
C-O _{ax}	1.151	1.151	1.133
Ru-C _{eq}	1.944	1.943	1.921
Ru...O _{eq}	3.093	3.093	3.048
C-O _{eq}	1.150	1.150	1.127
Angles			
Ru-Ru-Ru	60.00	60.00	60.00
Ru-Ru-C _{eq}	99.99	100.18	97.95
C _{eq} -Ru-C _{eq}	101.63	101.48	104.09
Ru-Ru-C _{ax} (acute)	78.98	78.53	88.99
Ru-Ru-C _{ax} (obtuse)	95.29	95.91	90.08
C _{ax} -Ru-C _{eq}	92.07	92.01	90.34
C _{ax} -Ru-C _{ax}	173.45	173.65	178.33
Ru-C-O _{ax}	173.01	172.67	172.98
Ru-C-O _{eq}	177.63	177.64	178.91
Dihedral Angles			
C _{eq} -Ru-Ru-C _{eq}	24.11	25.74	na
C _{ax} -Ru-Ru-C _{ax}	28.72	30.70	na

^aSee theoretical methods section (IID) for basis set information. ^bref 5

Table S2. Calculated vibrational frequencies (cm^{-1}) and relative amplitudes for the parent complex, $\text{Ru}_3(\text{CO})_{12}$, and the metal-metal cleavage complex, **I**.

$\text{Ru}_3(\text{CO})_{12}$		Complex I			
<i>Basis Set A</i> Unsolv.	<i>Basis Set B</i> Unsolv.	<i>Basis Set B</i> Unsolv.	Unsolv. ^a	Propane	THF ^c
1988 (0.01)	1995 (0.11)	1840 (0.39)	1859 (0.34)	1847 (0.27)	1838 (0.19)
2007 (0.08)	2002 (0.02)	1977 (0.01)	1984 (0.01)	1980 (0.02)	1975 (0.01)
2015 (0.03)		1989 (0.07)	1990 (0.08)	1988 (0.14)	1979 (0.25)
2024 (0.61)	2015 (0.60)	1997 (0.19)	1997 (0.16)	1992 (0.18)	1983 (0.10)
2047 (1.00)	2038 (1.00)	2007 (0.43)	2009 (0.07)	2012 (0.04)	2002 (0.01)
		2014 (0.11)	2017 (0.51)	2018 (0.14)	2008 (0.21)
		2022 (1.00)	2024 (0.12)	2024 (0.24)	2012 (0.23)
		2029 (0.12)	2031 (1.00)	2032 (1.00)	2024 (1.00)
		2036 (0.38)	2042 (0.35)	2039 (0.55)	2031 (0.45)
		2069 (0.37)	2048 (0.09)	2062 (0.00)	2035 (0.02)
		2101 (0.03)	2076 (0.36)	2076 (0.24)	2069 (0.15)
			2109 (0.04)	2116 (0.02)	2100 (0.00)

^a Unless otherwise specified, basis set A was used for all calculations. ^b THF solvated complexes are solvated by the oxygen atom of the THF molecule.

Table S3. Calculated vibrational frequencies (cm^{-1}) and relative amplitudes for the carbonyl loss complexes II_{ax} and II_{eq} .

Complex II_{ax}				Complex II_{eq}			
<i>Basis Set B</i> Unsolv.	Unsol. ^a	Propane	THF ^b	<i>Basis Set B</i> Unsolv.	Unsolv.	Proane	THF ^b
1862 (0.18)	1884 (0.18)	1879 (0.21)	1886 (0.16)	1940 (0.11)	1963 (0.06)	1967 (0.31)	1957 (0.04)
1948 (0.09)	1954 (0.11)	1957 (0.10)	1926 (0.14)	1966 (0.20)	1981 (0.25)	1982 (0.18)	1971 (0.16)
1972 (0.11)	1986 (0.11)	1984 (0.10)	1975 (0.07)	1973 (0.18)	1986 (0.15)	1986 (0.15)	1975 (0.12)
1994 (0.16)	2005 (0.37)	2003 (0.47)	1993 (0.22)	1986 (0.05)	1999 (0.06)	1994 (0.10)	1985 (0.17)
1996 (0.39)	2008 (0.19)	2004 (0.22)	1995 (0.24)	1991 (0.07)	2004 (0.07)	2002 (0.04)	1993 (0.05)
2008 (0.14)	2020 (0.16)	2019 (0.12)	2009 (0.12)	2001 (0.05)	2013 (0.06)	2010 (0.05)	2003 (0.02)
2012 (0.14)	2023 (0.11)	2023 (0.12)	2012 (0.07)	2013 (0.74)	2021 (0.88)	2017 (0.88)	2009 (0.80)
2022 (1.00)	2032 (1.00)	2032 (1.00)	2021 (0.39)	2021 (0.18)	2030 (0.13)	2026 (0.23)	2016 (0.40)
2026 (0.41)	2036 (0.40)	2034 (0.51)	2023 (1.00)	2024 (1.00)	2035 (1.00)	2034 (1.00)	2026 (1.00)
2043 (0.86)	2052 (0.88)	2050 (0.94)	2041 (0.79)	2037 (0.74)	2047 (0.77)	2044 (0.73)	2035 (0.79)
2086 (0.07)	2091 (0.07)	2090 (0.09)	2082 (0.10)	2088 (0.05)	2094 (0.04)	2092 (0.07)	2085 (0.08)

^a Unless otherwise specified, basis set A was used for all calculations. ^b THF solvated complexes are solvated by the oxygen atom of the THF molecule.

